# π-Radical to σ-Radical Tautomerization in One-Electron-Oxidized 1-Methylcytosine and Its Analogs

7 AUTHORS, INCLUDING:

Amitava Adhikary
Oakland University
43 PUBLICATIONS    701 CITATIONS

SEE PROFILE

Anil Kumar
Oakland University
59 PUBLICATIONS    1,156 CITATIONS

SEE PROFILE

Ragda M. Hindi
Oakland University
2 PUBLICATIONS    2 CITATIONS

SEE PROFILE

Michael D Sevilla
Oakland University
222 PUBLICATIONS    6,323 CITATIONS

SEE PROFILE

# π-Radical to σ-Radical Tautomerization in One-Electron-Oxidized 1-Methylcytosine and Its Analogs

Amitava Adhikary,* Anil Kumar, Casandra T. Bishop, Tyler J. Wiegand, Ragda M. Hindi, Ananya Adhikary, and Michael D. Sevilla*

Department of Chemistry, Oakland University, Rochester, Michigan 48309, United States

**S** *Supporting Information*

**ABSTRACT:** In this work, iminyl σ-radical formation in several one-electron-oxidized cytosine analogs, including 1-MeC, cidofovir, 2′-deoxycytidine (dCyd), and 2′-deoxycytidine 5′-monophosphate (5′-dCMP), were investigated in homogeneous, aqueous ($D_2O$ or $H_2O$) glassy solutions at low temperatures by employing electron spin resonance (ESR) spectroscopy. Upon employing density functional theory (DFT) (DFT/B3LYP/6-31G* method), the calculated hyperfine coupling constant (HFCC) values of iminyl σ-radical agree quite well with the experimentally observed ones, thus



Neutral aminyl radical
$C(N4-H)\bullet)_{anti}$
0.0 kcal/mol

$C(N4-H)\bullet)_{syn}$
-5.50 kcal/mol

Iminyl σ−radical
-9.01 kcal/mol

π-cation radical

confirming its assignment. ESR and DFT studies show that the cytosine iminyl σ-radical is a tautomer of the deprotonated cytosine π-cation radical [cytosine π-aminyl radical, C(N4−H)•]. Employing 1-MeC samples at various pHs ranging from ca. 8 to 11, ESR studies show that the tautomeric equilibrium between C(N4−H)• and the iminyl σ-radical at low temperature is too slow to be established without added base. ESR and DFT studies agree that, in the iminyl σ-radical, the unpaired spin is localized on the exocyclic nitrogen (N4) in an in-plane pure p-orbital. This gives rise to an anisotropic nitrogen hyperfine coupling ($A_{zz} = 40$ G) from N4 and a near isotropic β-nitrogen coupling of 9.7 G from the cytosine ring nitrogen at N3. Iminyl σ-radical should exist in its N3-protonated form, as the N3-protonated iminyl σ-radical is stabilized in solution by over 30 kcal/mol ($\Delta G = -32$ kcal/mol) over its conjugate base, the N3-deprotonated form. This is the first observation of an isotropic β-hyperfine ring nitrogen coupling in an N-centered DNA radical. Our theoretical calculations predict that the cytosine iminyl σ-radical can be formed in double-stranded DNA by a radiation-induced ionization−deprotonation process that is only 10 kcal/mol above the lowest energy path.
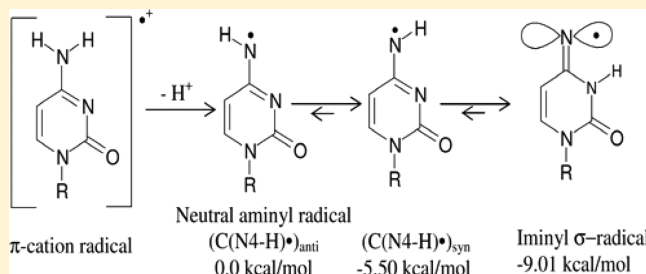
## INTRODUCTION

High-energy radiation impinging on DNA causes random ionization events in approximate proportion to the number of valence electrons present at any DNA site. Thus, formation of holes takes place at each of the bases as well as at the sugar−phosphate backbone, forming G•+, A•+, C•+, T•+, and [sugar−phosphate]•+.[1−8] Both purine and pyrimidine base cation radicals have been extensively studied experimentally in aqueous solution at room temperature by pulse radiolysis and flash photolysis as well as by electron spin resonance (ESR) at low temperatures in monomers, oligomers of defined sequences, polynucleotides, and in highly polymeric DNA (e.g., salmon sperm, calf thymus).[1−14] The mechanistic pathways of formation of DNA damage products from these initially produced cation radicals are critically influenced by the electronic nature (π or σ) of the DNA radicals. Calculations employing density functional theory (DFT) predict that formation of both π- or σ-type DNA cation radicals may be observed in DNA bases and analogs.[15] The DNA base cation radicals, G•+, A•+, C•+, and T•+, have been found to be only π-type cation radicals in irradiated DNA and its model systems.[7,15] DFT calculations, however, predict that the σ-states for one-electron-oxidized pyrimidine DNA bases are

energetically close to the corresponding lower-lying π-states.[15] Experimental evidence on formation of σ-type radicals has been presented in one-electron-oxidized pyrimidine derivatives having modified nucleobases (e.g., 2-thiothymine,[16] 6-azauracil, 6-azathymine, and 6-azacytosine[17]).

For cytosine base π-cation radical (C•+) produced via one-electron oxidation by $SO_4^{•−}$ in monomers, pulse radiolysis studies have suggested that deprotonation from the exocyclic amine group to the surrounding solvent (Scheme 1) leads to the formation of a neutral cytosine π-aminyl radical [C(N4−H)•].[9,18,19] Time-resolved ESR studies of 1-methylcytosine (1-MeC) in $H_2O$ by Beckert et al. had presented evidence of the 1-MeC π-cation radical formation by electron transfer from 1-MeC to the triplet state of anthraquinone-2,6-disulfonate.[20] The 1-MeC π-cation radical subsequently deprotonated to the π-aminyl radical [1-MeC(N4−H)•], which showed a 17.4 G doublet from the exocyclic N−H proton; further confirmation of this assignment came from studies in $D_2O$, where this doublet collapsed owing to the exchangeable nature of the

**Scheme 1. Formation of Cytosine π-Cation Radical via One-Electron Oxidation of Cytosine Monomers**[a]
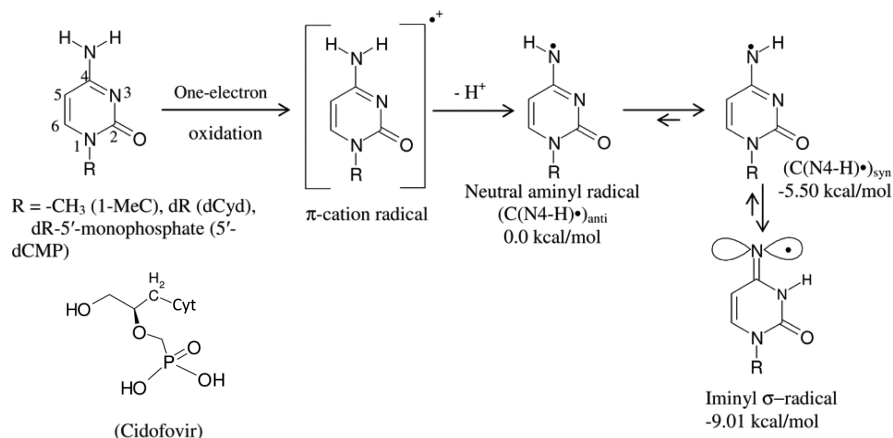


[a]The cytosine π-cation radical, via deprotonation and subsequent tautomerization, leads to the formation of iminyl radical, which is a σ-radical by nature. The atom numbering scheme of the cytosine base is shown. The relative stabilities of C(N4−H)•$_{syn}$, C(N4−H)•$_{anti}$, and iminyl σ-radical in kcal/mol are provided. Optimization of the geometries of these radicals along with their energy values employing optimized structures were obtained with the aid of the DFT/B3LYP/6-31G* method.

exocyclic N−H proton.[20] Furthermore, pulse radiolysis studies in aqueous solutions of SeO$_3$•−-mediated one-electron-oxidized calf thymus DNA have proposed that σ-iminyl radical from cytosine could be as an intermediate to guanine cation radical formation.[21]

Steady-state or continuous-wave ESR (CW ESR) studies using 1-MeC as a model of a cytosine monomer[9,19] have suggested that the neutral π-aminyl radical formed by deprotonation of the π-cation radical led to subsequent radical production. The experimentally obtained hyperfine coupling constant (HFCC) values of this new radical were compared to those of DFT-calculated nitrogen and hydrogen HFCC for several aminyl and iminyl radicals.[9,19] This comparison of HFCC values led to the tentative assignment of the new radical species to the iminyl σ-radical,[9,19] which is a tautomer of the neutral π-aminyl radical (Scheme 1). This tentative assignment has not been confirmed to date.

Various cytosine analogs [e.g., 1-MeC, cidofovir, the nucleoside 2′-deoxycytidine (dCyd), and the nucleotide (5′-dCMP)] are investigated in this work. Electron spin resonance (ESR) spectroscopic studies show formation of the iminyl σ-radical (Scheme 1) in these one-electron-oxidized cytosine analogs in homogeneous aqueous (D$_2$O or H$_2$O) glassy solutions at low temperatures and at higher pH (ca. 10 and above). Calculations employing density functional theory (DFT) support the ESR spectral assignment of the iminyl σ-radical. These results clearly show that the cytosine iminyl σ-radical is a tautomer of the neutral cytosine π-aminyl radical, C(N4−H)• (Scheme 1) and that the C(N4−H)• formation occurs through deprotonation of the cytosine base π-cation radical at the exocyclic amine (Scheme 1). The combination of ESR studies and DFT calculations identifies both species [C(N4−H)• and cytosine iminyl σ-radical] involved in the tautomeric equilibria. At low temperature, the shift in the tautomeric equilibria to the cytosine iminyl σ-radical is aided by the presence of a proton acceptor, for example, −OH. These results show that the unpaired spin in the iminyl σ-radical is localized to the exocyclic nitrogen (N4) in an in-plane pure p-orbital, which gives rise to an anisotropic nitrogen hyperfine coupling from N4 and a near isotropic β-hyperfine coupling from the nitrogen (N3) on the cytosine ring. Previous spin-

trapped DNA radicals have shown nitrogen couplings that are β to the nitroxide nitrogen.[22] However, this is the first example of near isotropic β-hyperfine ring nitrogen coupling in a DNA base radical itself. In addition, theoretical calculations are employed to clarify the reaction energies of iminyl σ-radical-induced oxidation of G in a one-electron-oxidized G:C base pair.

## MATERIALS AND METHODS

**Compounds.** 1-Methylcytosine (1-MeC, Scheme 1) and 2′-deoxycytidine (dCyd) were obtained from Sigma Chemical Co. (St. Louis, MO). 1-MeC was also procured from Astatech Inc. (Bristol, PA). Cidofovir (Scheme 1) was purchased from ADooQ Bioscience (Irvine, CA). Lithium chloride (LiCl) [ultra dry, 99.995% (metals basis)] and 2′-deoxycytidine 5′-monophosphate (5′-dCMP) were purchased from Alfa Aesar (Ward Hill, MA). Deuterium oxide (D$_2$O) (99.9 atom % D) was purchased from Aldrich Chemical Co. Inc. (Milwaukee, WI). Potassium persulfate (K$_2$S$_2$O$_8$) was procured from Mallinckrodt, Inc. (Paris, KY). All compounds were used without further purification.

**Glassy Sample Preparation.** As per our ongoing studies on various model systems of DNA and RNA,[7,8,23−35] the homogeneous glassy samples of 1-MeC, cidofovir, dCyd, and 5′-dCMP were prepared as follows:

*A. Preparation of Homogeneous Solutions.* Homogeneous solutions were prepared by dissolving 0.6−9.8 mg/mL of the compound in 7.5 M LiCl in either D$_2$O or H$_2$O and in the presence of K$_2$S$_2$O$_8$ (6−20 mg/mL). K$_2$S$_2$O$_8$ was added as an electron scavenger so that only the formation of the one-electron-oxidized species and its subsequent reactions can be followed employing ESR spectroscopy.

*B. pH Adjustments.* The pH of these homogeneous solutions either in 7.5 M LiCl/D$_2$O or in 7.5 M LiCl/H$_2$O was adjusted to the range of ca. 8−11. These pH adjustments were performed by quickly adding microliter amounts of 1 M NaOH under ice-cold conditions. Owing to the high ionic strength (7.5 M LiCl), pH meters would not provide accurate pH measurements of these solutions. Hence, pH papers were employed to measure the pH values of these solutions, and these pH values are approximate.

*C. Preparation of Glassy Samples and Their Storage.*
These pH-adjusted homogeneous solutions were thoroughly bubbled with nitrogen gas. These solutions were then immediately drawn into 4 mm Suprasil quartz tubes (Catalog no. 734-PQ-8, WILMAD Glass Co., Inc., Buena, NJ). By rapidly immersing the quartz tubes containing these solutions in liquid nitrogen (77 K), these solutions were cooled to 77 K. As a result of the rapid cooling at 77 K, the homogeneous liquid solutions form transparent homogeneous glassy solutions. For $\gamma$-irradiation and subsequent progressive annealing experiments, these homogeneous, glassy solutions were used. All glassy samples were stored at 77 K in Teflon containers in the dark.

**$\gamma$-Irradiation of Glassy Samples and Their Storage.**
Following our ongoing efforts to generate various DNA and RNA model systems,[8,23−35] the glassy samples were $\gamma$ ($^{60}$Co)-irradiated (absorbed dose = 1.4 kGy) at 77 K and stored at 77 K in Teflon containers in the dark.

**Annealing of Glassy Samples.** We have employed a variable-temperature assembly that passed liquid-nitrogen-cooled dry nitrogen gas past a thermistor and over the sample for the annealing as per our previous studies.[8,23−35] Each glassy sample has been progressively annealed in the range of 140−170 K for 15 min. The matrix radical $Cl_2^{\bullet -}$ causes one-electron oxidation of the solute (e.g., 1-MeC) via annealing and thus enables us to study only the solute cation radical production and its subsequent reactions directly via ESR spectroscopy.

**Electron Spin Resonance.** As per our ongoing studies on DNA and RNA radicals,[7,8,23−35] a Varian Century Series X-band (9.3 GHz) ESR spectrometer with an E-4531 dual cavity, 9-in. magnet, and a 200 mW Klystron was used, and Fremy's salt ($g_{center}$ = 2.0056, $A(N)$ = 13.09 G) was employed for the field calibration. All ESR spectra have been recorded at 77 K and at 40 dB (20 $\mu$W). Spectral recording at 77 K maximizes signal height and allows for comparison of signal intensities.

Following our works on DNA and RNA radicals,[7,8,23−35] the anisotropic simulations of the experimentally recorded ESR spectra were carried out by employing the Bruker programs WIN-EPR and SimFonia. The ESR parameters [e.g., hyperfine coupling constant (HFCC) values, line width] were adjusted to obtain the "best fit" simulated spectrum that matched the experimental ESR spectrum well (see Figure S1 of the Supporting Information and our other work[26,28,29,35]).

**Calculations Based on DFT.** B3LYP functional and 6-31G* as the basis set implemented in the Gaussian 09 suit of program[36] have been employed to carry out the theoretical calculations, such as geometry optimizations and calculations of the HFCC values of radicals in 1-MeC (see the Supporting Information). The calculated HFCC values employing the B3LYP/6-31G* method agree well with those obtained using experiment.[7,8,10,23−35,37] The GaussView[38] program was used to plot the spin densities and molecular structures.

For localization of the radical site of cytosine iminyl $\sigma$-radical in one-electron-oxidized G:C base pair, the DFT/$\omega$b97x/6-31++G(d) method was employed for geometry optimization to study the reaction energies along with spin density distribution plots. The integral equation formalism polarized continuum model[39] (IEF-PCM) as implemented in Gaussian 09 was used to treat the effect of full solvent. The group of Head-Gordon developed the $\omega$b97x functional,[40,41] and this functional was observed to be very successful for the calculations of various properties of molecules in different spin states.[35,42]

## ■ RESULTS AND DISCUSSION

**ESR Studies.** *Formation of the Iminyl $\sigma$-Radical in One-Electron-Oxidized 1-MeC, Cidofovir, dCyd, and 5′-dCMP.* In Figure 1, we present the ESR spectral (spectra recorded at 77
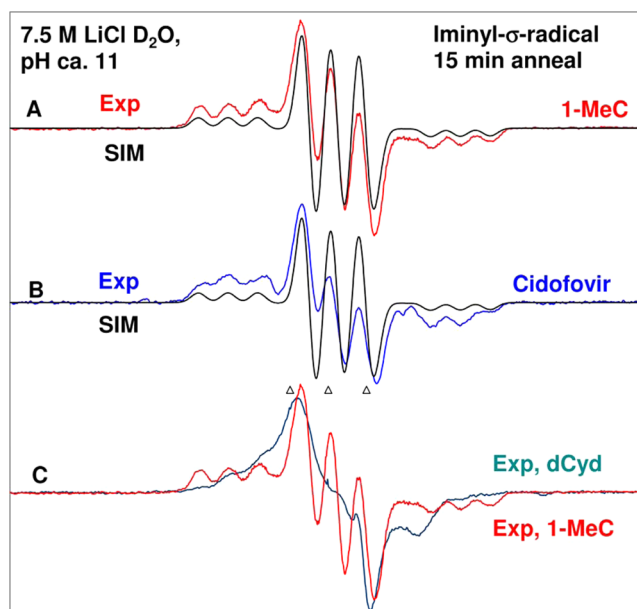


**Figure 1.** ESR spectra of iminyl $\sigma$-radical formed in $\gamma$-irradiated (dose = 1.4 kGy at 77 K) matched glassy samples (2 mg/mL each) of (A) 1-MeC (red), (B) cidofovir (blue), and (C) dCyd (teal) in 7.5 M LiCl/D$_2$O with the electron scavenger K$_2$S$_2$O$_8$ (8 mg/mL in each sample), pH ca. 11, via annealing at 160−165 K for 15 min after one-electron oxidation of the cytosine base by $Cl_2^{\bullet -}$. The simulated spectra (black) due to iminyl $\sigma$-radical of one-electron-oxidized 1-MeC (A) and cidofovir (B) are placed underneath the experimental spectra. For simulation parameters, see the text. (C) The experimentally recorded spectrum of one-electron-oxidized dCyd (teal). The experimentally obtained iminyl $\sigma$-radical spectrum from 1-MeC (red, part A) has been superimposed on this spectrum for comparison. All ESR spectra shown in parts A−C were recorded at 77 K. The three reference markers in this figure and in subsequent figures are Fremy's salt resonances with the central marker at $g$ = 2.0056 and each of three markers is separated from one another by 13.09 G.

K) evidence showing formation of the iminyl $\sigma$-radical in matched homogeneous glassy (7.5 M LiCl in D$_2$O) samples of one-electron-oxidized 1-MeC, cidofovir, dCyd, and 5′-dCMP. We note here that cidofovir, a cytosine nucleotide analog (Scheme 1), is an antiviral agent that is widely used to treat cytomegalovirus infection in the retina of patients with AIDS.[43,44]

The ESR spectrum (red) from a $\gamma$-irradiated (absorbed dose = 1.4 kGy, $\gamma$-irradiation at 77 K) homogeneous glassy (7.5 M LiCl/D$_2$O, pH ca. 11) sample of 1-MeC (2 mg/mL) in the presence of K$_2$S$_2$O$_8$ as electron scavenger obtained via annealing at 165 K for 15 min in the dark is presented in Figure 1A. The spectra from matched samples of cidofovir (blue) and dCyd (teal) also at pH ca. 11 are presented in parts B and C of Figure 1, respectively. The ESR spectra obtained from matched samples of 1-MeC (pH ca. 10) and cidofovir (pH ca. 11) via progressive annealing in the dark and in the temperature range from 77 K (immediately after $\gamma$-irradiation at 77 K) to 170 K are presented in the Supporting Information (Figures S2−S7).

**Table 1. Comparison of Experimentally Obtained HFCCs Values of the Iminyl $\sigma$-Radical and C(N4−H)$^\bullet$ (in gauss, G) with Those Obtained by Calculation Using the DFT/B3LYP/6-31G* Method**

| | | | | HFCC (G) | | | | | | | | |
| | | | | theory | | | | | | | expl[a] | |
| | | | | | $A_{aniso}$ | | | $A_{total}$[a,b] | | | $A_{total}$[a,b,c] | | |
| molecule | radical | atoms | $A_{iso}$ | $A_{xx}$ | $A_{yy}$ | $A_{zz}$ | $A_{xx}$ | $A_{yy}$ | $A_{zz}$ | $A_{xx}$ | $A_{yy}$ | $A_{zz}$ |
|---|---|---|---|---|---|---|---|---|---|---|---|---|
| 1-MeC | iminyl $\sigma$-radical | N4 atom | 11.6 (11.7[d]) | 26.2 | −11.2 | −15.1 | 37.2 | 0.4 | −3.5 | 40 | 0 | 0 |
| | | N3 atom | 12.4 (12.3[d]) | 1.9 | −0.6 | −1.3 | 14.3 | 11.8 | 10.9 | 10.2 | 9.5 | 9.5 |
| | | H3 atom | 0.8 (0.8[d]) | 3.8 | −1.2 | −2.6 | 4.6 | −0.4 | −1.8 | nd | nd | nd |
| 1-MeC | C(N4−H)$^\bullet_{syn}$ | N4 atom | 10.7 (10.8[d]) | 21.6 | −10.7 | −10.9 | 32.3 | 0.0 | −0.2 | 28.0 | 0 | 0[e] |
| | | N3 atom | 4.3 (3.7[d]) | 8.1 | −4.2 | −3.9 | 12.4 | 0.1 | 0.4 | 10.5 | 0 | 0[e] |
| | | H4 atom | −17.6 | −3.8 | 16.9 | −13.2 | −20.8 | −0.7 | −30.8 | | | |
| | C(N4−H)$^\bullet_{anti}$ | N4 atom | 10.5 | 21.44 | −10.9 | −10.5 | 31.94 | −0.4 | 0 | 28.0 | 0 | 0[e] |
| | | N3 atom | 4.9 | 9.6 | −4.9 | −4.7 | 14.5 | 0 | 0.2 | 10.5 | 0 | 0[e] |
| | | H4 atom | −17.7 | −3.6 | 17.6 | −13.9 | −21.3 | −0.1 | −31.6 | | | |

[a]Experiments give the magnitude but not the sign of the couplings. Estimated errors are of ±1 G for $A_{zz}$, $A_{xx}$, and $A_{yy}$. See the Supporting Information (Figure S1) for details. [b]$A_{total} = A_{iso} + A_{aniso}$. [c]nd = not detected [d]ref 19 reports only isotropic HFCC values, which are shown in parentheses. [e]The experimental spectrum (pink) in Figure 2A is analyzed to obtain the experimental values of $A_{zz}$ components of the nitrogen hyperfine couplings.

Following our ongoing work on formation of one-electron-oxidized species by $Cl_2^{\bullet-}$ in DNA model structures,[8,23−32,34,35] progressive annealing of these samples at and above 140 K softens the glass so that the migration of $Cl_2^{\bullet-}$ and its reaction with the solute, for example, 1-MeC, produces only one-electron-oxidized 1-MeC. Therefore, spectrum 1A (red) has been obtained after further annealing of one-electron-oxidized 1-MeC sample at 165 K. In other words, the spectrum obtained in Figure 1A is due to a radical species that is produced from the 1-MeC π-cation radical or its deprotonated species, i.e., π-aminyl radical [1-MeC(N4−H)$^\bullet$]. Employing pulse radiolysis in aqueous solution at ambient temperature, the p$K_a$ of the cytosine π-cation radical (C$^{\bullet+}$) in dCyd has been reported as 4.[12] Also, theoretically (DFT) predicted p$K_a$ values of C$^{\bullet+}$ in dCyd are 3.4[45] and 3.6−4.2,[46] the latter being more accurate. Since C$^{\bullet+}$ produces C(N4−H)$^\bullet$ by fast, reversible deprotonation from the exocyclic amine group (Scheme 1),[9,18−20,45,46] the radical observed in Figure 1 after annealing at 165 K and at pH 10 and above should be produced from C(N4−H)$^\bullet$ (Scheme 1), which is supported by our results in Figure 2. We have assigned this radical species as iminyl σ-radical (Scheme 1). Justification of this radical assignment is provided below.

*Assignment of Spectra in Figure 1A to the Iminyl σ-Radical in 1-MeC.* It is evident from the hyperfine splittings, line intensities, and g-value of the experimentally obtained spectrum (red) shown in Figure 1A that this ESR spectrum results in two nitrogen HFCC values: one anisotropic N atom HFCC and one nearly isotropic N atom HFCC. This spectrum has been simulated by employing the ESR parameters ($A_{xx}$, $A_{yy}$, and $A_{zz}$) for two nitrogens as (40.0, 0, 0) and (10.2, 9.5, 9.5) G, along with $g_{xx}$, $g_{yy}$, $g_{zz}$ values of 2.0023, 2.0043, 2.0043, an isotropic line width of 5 G, and a mixed Lorentzian/Gaussian = 1. The simulated spectrum (black) is superimposed on the experimentally obtained spectrum (blue) in Figure 1A and both spectra match nicely. Our DFT calculations show that these couplings are in agreement only with an iminyl σ-radical (vide infra).

The experimental and theoretical work by von Sonntag et al.[9,19] for the CW ESR spectrum of $SO_4^{\bullet-}$-induced one-electron-oxidized 1-MeC in aqueous solution at room temperature had presented an isotropic g-value (2.0035) indicative of a N-centered radical and the fit of DFT calculations of N atom isotropic hyperfine couplings to their experimental values [$A_{iso}$(N3) = 11.8 G; $A_{iso}$(N4) = 11.6 G].[19] We also note here that the isotropic HFCC values of the nitrogen with a radical site in other iminyl radicals [e.g., 9-fluorenoneiminyl radical (9.7 G)[47] and dialkyl as well as diaryl iminyl radical (9.1−10.3 G)[48]] measured in aqueous solutions at ambient temperature are quite close to the isotropic HFCC value of the nitrogen with a radical site ($A_{iso}$(N3) = 11.8 G) observed by von Sonntag et al.[19] These agreements led von Sonntag et al.[19] to the tentative assignment of this N-centered radical to the iminyl σ-radical (Scheme 1). This previous work is in accord with our assignment of the spectrum in Figure 1A to the iminyl σ-radical (Scheme 1). Indeed, the isotropic components of the HFCC values from our work are 13.3 G (N4) and 9.7 G (N3) (see Table 1) with an isotropic g-value of 2.0036. Considering the different media (homogeneous glassy solutions at low temperatures (our work) vs aqueous solution at room temperature (von Sonntag et al.[9,19]), the isotropic components of the HFCC values as well as the isotropic g-value from our work compare very well with those of von Sonntag et al.[9,19]

From the structural formula of the iminyl σ-radical (Scheme 1), it is evident that the N3 atom is in a β-position to the p-orbital at the radical site on the N4 atom and should give an isotropic N atom HFCC value, as seen in the spectrum shown in Figure 1A. We note here that there are reported nitrogen couplings that are β to the nitroxide nitrogen in spin-trapped DNA radicals;[22] however, the nearly isotropic β-nitrogen HFCC in this iminyl σ-radical is the only β nitrogen coupling that is reported to date in a DNA radical itself. This iminyl σ-radical assignment is aptly supported by DFT calculations (vide infra).

*Formation of Iminyl σ-Radical in Cidofovir, dCyd, and 5′-dCMP.* To investigate whether the cytosine iminyl σ-radical production is affected by the nature of the side chain at N1 of the cytosine base (Scheme 1), we have employed matched samples of one-electron-oxidized cidofovir, dCyd, and 5′-dCMP in homogeneous aqueous glassy solution [7.5 M LiCl/$D_2O$ (or LiCl/$H_2O$)] at pH 10 and above and have progressively annealed these samples up to ca. 160−165 K.

These results are presented in parts B and C of Figure 1, respectively, for cidofovir and dCyd (see Supporting Information Figures S5 and S6 for cidofovir and Figure S7 for 5′-dCMP).

A simulated spectrum (black) using the same nitrogen HFCC values and g-values as employed for 1-Me-C iminyl σ-radical in Figure 1A is superimposed on the experimentally obtained spectrum (blue) in Figure 1B, and both spectra match nicely. Hence, the spectra in Figure 1B are also assigned to the cidofovir iminyl σ-radical (Scheme 1).

The experimentally recorded spectrum of one-electron-oxidized dCyd (teal) is shown in Figure 1C. The experimentally obtained iminyl σ-radical spectrum from 1-MeC (red, Figure 1A) has been superimposed on this spectrum for comparison. It is evident from both spectra shown in Figure 1C that spectrum obtained from the one-electron-oxidized dCyd sample has the same hyperfine components as the iminyl σ-radical spectrum from 1-MeC but is overlapped with a broad underlying spectrum that we assign to dCyd C(N4−H)$^•$, the untautomerized precursor of the iminyl σ-radical (see Figure 2A for the spectrum of C(N4−H)$^•$, the π-radical for 1-MeC, and Figure 2B for a similar case of overlap of the iminyl σ-radical over the broad π-radical). Hence, the spectrum of one-electron-oxidized dCyd (teal) in Figure 1C is assigned to the dCyd iminyl σ-radical overlapped with dCyd (N4−H)$^•$ (Scheme 1). Similar results were found by employing the matched sample of 5′-dCMP; these results are presented in the Supporting Information (Figure S7).

We note that the N3−H proton would show only small HFCC values of ca. 2 G in the iminyl σ-radicals (see Table 1 and Supporting Information). Since this proton is exchanged in the D$_2$O system, the coupling is reduced by a factor of 6.514; thus, the N3-D does not contribute to the iminyl σ-radical spectrum.

*pH Dependence on the Iminyl σ-Radical Formation.* It is evident from Figure 1 that the 1-MeC iminyl σ-radical spectrum shows excellent resolution of the line components. Therefore, it is of interest to see the precursor radicals after one-electron oxidation. So, the effect of pH on the iminyl σ-radical formation has been investigated by employing matched samples of 1-MeC in homogeneous 7.5 M LiCl/D$_2$O glassy solutions with pH values of ca. 8, 9.5, and 11. The spectra of these samples are presented in Figure 2.

In Figure 2A, the experimentally recorded (77 K) ESR spectrum (pink) of one-electron-oxidized 1-MeC at pH (pD) ca. 8 in a homogeneous glassy 7.5 M LiCl/D$_2$O solution is shown. Following our results in Figure 1, the one-electron oxidation of 1-MeC at pH ca. 8 was induced by Cl$_2^{•−}$ attack after annealing at 160 K in the dark.

The experimentally recorded spectra obtained from matched samples of one-electron-oxidized 1-MeC at pD ca. 9.5 (blue spectrum) and at ca. 11 (red spectrum) are shown in Figure 2B,C. The spectrum of one-electron-oxidized 1-MeC sample at pH ca. 11 was found to be identical to that shown in Figure 1A. Therefore, the experimentally recorded spectrum (red) in Figure 1A is shown here as Figure 2C. The simulated spectra in black (Figure 2A,C) are presented along with the experimentally recorded spectra. The experimentally recorded as well as the simulated spectra in Figure 2C are assigned to the same species, the iminyl σ-radical (see Figure 1).

The blue spectrum in Figure 2A is best-matched with a simulated spectrum that has been obtained by employing two anisotropic $^{14}$N (nuclear spin = 1) HFCC values of (28.0, 0, 0)
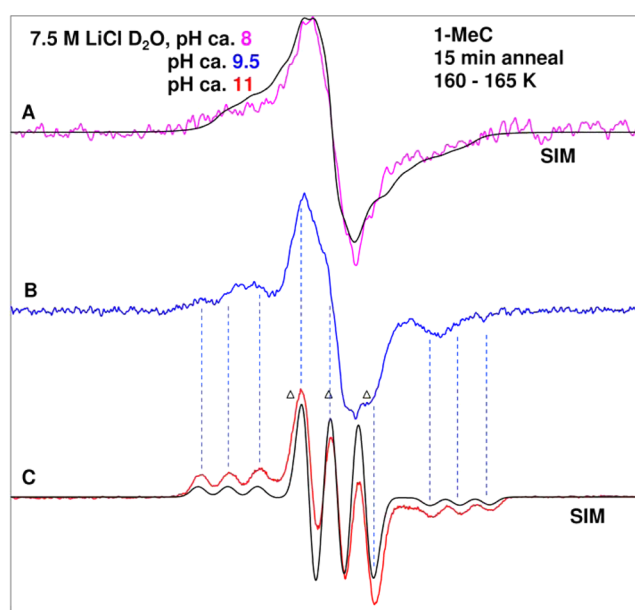


**Figure 2.** ESR spectra obtained from matched 1-MeC samples (concentration of 1-MeC in each sample = 2 mg/mL in 7.5 M LiCl/D$_2$O) in the presence of the electron scavenger K$_2$S$_2$O$_8$ (8 mg/mL in each sample). Each sample has been γ-irradiated (absorbed dose = 1.4 kGy at 77 K), subsequently annealed to 160−165 K for 15 min in the dark at various pHs: (A) pH ca. 8 (pink), (B) pH ca. 9.5, and (C) pH ca. 11 (red, spectrum in Figure 1C). The simulated spectra (black) due to the π-aminyl radical [1-MeC(N4−H)$^•$] in part A as well as owing to the iminyl σ-radical of one-electron-oxidized 1-MeC in part C are respectively placed underneath the experimental spectra. The line components of the red (or black) spectrum in part C are visible in part B (see dotted lines). See the text for the details of simulation. All ESR spectra are recorded at 77 K.

and (10.5, 0, 0) G, a deuterium coupling of (3.8, 0, 5.5) G, and $g_{xx}$, $g_{yy}$, $g_{zz}$ (2.0019, 2.0047, 2.0047), along with an isotropic Gaussian line width of 4.5 G. The simulation shows that the deuterium coupling only contributes to the broadening of the spectrum. The simulated spectrum in black is superimposed on the experimentally recorded spectrum in Figure 2A, and both spectra match reasonably well. The radical species giving rise to Figure 2A is assigned to the neutral aminyl π-radical C(N4−H)$^•$, which is the precursor to the 1-MeC iminyl σ-radical (Scheme 1). Our DFT calculations show two anisotropic nitrogen HFCC values for C(N4−H)$^•_{syn}$ that agree well with experiment (see the pink spectrum in Figure 2A, Table 1, and the theory section).

Comparison of the experimentally recorded spectrum of one-electron-oxidized 1-MeC sample (blue, pH ca. 9.5) in Figure 2B with that of the 1-MeC iminyl σ-radical spectrum (red, pH ca. 11) in Figure 2C shows that the blue spectrum contains line components of the iminyl σ-radical spectrum (see dotted lines, especially at the left wings and at the center), and computer subtraction shows that it accounts for approximately 30% of the overall intensity. Thus, we conclude that the spectrum 2B is a cohort of two radicals [ca. 70% C(N4−H)$^•_{syn}$ (Figure 2A) and ca. 30% iminyl σ-radical (Figure 2C)]

These results, therefore, clearly show that C(N4−H)$^•$ is the precursor to the 1-MeC iminyl σ-radical. Thus, both species C(N4−H)$^•$ and the iminyl σ-radical, which are in tautomeric equilibria (see Scheme 1), are identified. In our system, we observe only ca. 30% conversion of C(N4−H)$^•$ to the iminyl σ-radical at pH ca. 9.5 after annealing the sample in the range

160−165 K for 15 min in the dark. Therefore, comparison of the experimental and theoretical work by von Sonntag et al.[9,19] for the CW ESR spectrum of $SO_4^{\bullet-}$-induced one-electron-oxidized 1-MeC in aqueous solution (pH ca. 7) with the CW ESR spectral studies of $Cl_2^{\bullet-}$-induced one-electron-oxidized 1-MeC in our homogeneous glassy solutions at low temperatures at higher pH (Figures 1 and 2) clearly shows that the equilibrium between C(N4−H)• and the iminyl σ-radical at low temperature is too slow to be established without the base.

We note that our theoretical results predict that the iminyl σ-radicals do not undergo deprotonation at N3 (see theory).

*Subsequent Reaction of the Iminyl σ-Radical.* Iminyl radicals are highly reactive and well-known for undergoing various types of reactions, such as dimerization,[48] addition to double and triple bonds,[49] and H atom abstraction leading to DNA cleavage.[50] von Sonntag proposed that the iminyl radical of 1-methylcytosine undergoes dimerization.[9,19] We also note that in the work employing DFT calculations in the gas phase and in the presence of water, the cytosine iminyl σ-radical has been shown to be the key intermediate in deamination of cytosine to uracil that is mediated by cytosine base π-cation radical or its deprotonated form, C(N4−H)•.[51] Several alternative pathways have been suggested at room temperature in aqueous solutions. For example, C1′• formation and it is diamagnetic product 2-deoxyribonolactone were reported upon menadione-induced one-electron oxidation of dCyd due to type I photosensitization.[22,52] Also, in the same experiments, 6-hydroxy-5,6-dihydrocytosin-5-yl radical was reported to be the predominant radical via hydration of cytosine π-cation radical.[22,52,53]

The line intensities of the iminyl σ-radical spectrum in 1-MeC decrease by a factor of ca. 4 by progressive annealing from 160 to ca. 170 K (see the Supporting Information, Figure S4). We attribute this simple decay of line intensities to dimerization of the iminyl σ-radicals in 1-MeC.

Upon further annealing of matched cidofovir samples (0.6−9.8 mg/mL) to 170 or 175 K (see the Supporting Information, Figure S5), we find that the line components from the cidofovir iminyl σ-radical are decreased for samples with concentrations of 0.6 and 2 mg/mL but not much for a sample with a concentration of 9.8 mg/mL. Simultaneously, a spectrum consisting of one anisotropic α-hydrogen HFCC [(10.0, 22.0, 35.0) G] and one isotropic β-hydrogen HFCC (49.5 G), along with a g-value of (2.0042, 2.0020, 2.0049), was found to develop without loss of signal intensity for cidofovir samples at 2 and 9.8 mg/mL but not for the cidofovir sample at 0.6 mg/mL. The g-value of this multiplet spectrum is in accord with those of the C-centered radicals near heteroatoms.[2−4,7,8,35] This concentration-dependent formation of the C-centered radical ruled out a cidofovir iminyl σ-radical-induced deprotonation reaction similar to our recent findings of C3′• formation in gemcitabine[35] or by intramolecular H atom abstraction by the iminyl σ-radical either from the −CH₂−OH moiety or from the N1−CH₂− moiety on the cidofovir side chain (see Scheme 1). However, the concentration-dependent C-centered radical production points to a bimolecular addition of the iminyl σ-radical to the C5═C6 double bond of an unreacted proximate cidofovir molecule.

*Influence of the Solvent (D₂O vs H₂O) on Formation of the Iminyl σ-Radical in 1-MeC and Cidofovir.* Employing 1-MeC as well as cidofovir samples in H₂O instead of a D₂O glass (7.5 M LiCl/H₂O, pH ca. 10), ESR studies on formation of the iminyl σ-radical in one-electron-oxidized 1-MeC and cidofovir

were carried out to observe the effect of couplings from exchangeable proton sites. These results are presented in the Supporting Information (Figures S2, S3, and S6). The results in Figure S3 are compared with those obtained using a matched 1-MeC sample in D₂O glass. It is evident from Figures 1 and S2D, S3D, and S6C that these spectra are due to the iminyl σ-radical. Owing to the relatively softer nature of an H₂O glass than a D₂O glass, progressive warming of the 1-MeC and cidofovir samples in H₂O glass to 155 K results in the complete conversion of C(N4−H)• to the iminyl σ-radical (Figure 1), as found in D₂O glasses at 165 K.

It is evident from the spectral simulations for the iminyl σ-radical in Figures 1 and S2D, S3D, and S6C that the change of solvent (D₂O vs H₂O) causes observable line broadening (5 G in D₂O vs 7.5 G in H₂O) and affects line shape [mixed (Lorentzian/Gaussian = 1) for D₂O vs Gaussian in H₂O], but most importantly, the N atom hyperfine couplings [(40.0, 0, 0) and (10.2, 9.5, 9.5) G] and the g-values [$g_{xx}$, $g_{yy}$, $g_{zz}$ (2.0023, 2.0043, 2.0043)] remain unaltered. For the 1-MeC iminyl σ-radical, the DFT/B3LYP/6-31G*-predicted HFCC value of ca. 3 G for the exchangeable N3−H proton (Table 1) is less than the line width of 7.5 G and hence cannot be observed in the broad ESR spectrum (Figures S2 and S3). However, the exchangeable N3−H proton HFCC should contribute to the observed line broadening. Moreover, Figures S3D and S6C show the presence of outermost weak line components (outermost lines at ca. 127 G). These small components are from an unidentified species in low intensity and are not included in the simulation.

We conclude that the iminyl σ-radical is produced in H₂O systems as in D₂O with only line broadening of the ESR spectra. Thus, the change of solvent does not affect the reactions leading to formation of iminyl σ-radical shown in Scheme 1.

**Theoretical Studies.** *Cytosine Iminyl σ-Radical in 1-MeC.* In this DFT study, we have considered 1-MeC•+ (Scheme 1) along with three different tautomers of C(N4−H)• (Scheme 1): (i) deprotonation of 1-MeC•+ at either the syn or anti sites of the >C═O group at C2 with respect to the N4−H atom (Scheme 1), leading to the formation of C(N4−H)•, and (ii) iminyl σ-radical tautomer of C(N4−H)• (Scheme 1). The geometries of all these radicals were fully optimized by employing the B3LYP/6-31G* method in the gas phase (see the Supporting Information). The relative stabilities of the three different tautomers, C(N4−H)•_anti, C(N4−H)•_syn, and iminyl σ-radical were 0.00, −5.50, and −9.01 kcal/mol, respectively (Scheme 1). These calculations clearly predict that the iminyl σ-radical is the most stable radical species when compared to C(N4−H)•_syn and C(N4−H)•_anti. The stability (3.5 kcal/mol) of the iminyl σ-radical in comparison to C(N4−H)•_syn is in good agreement with that (2.5 kcal/mol) calculated by von Sonntag et al. by employing the UB3LYP/6-31G(d)/Onsagar SCRF method.[19] The experimentally determined HFCC values (see Figure 2) of C(N4−H)• match very well with the predicted HFCC values of C(N4−H)•_syn.

It is evident from Table 1 that our calculated isotropic HFCC values of 1-MeC iminyl σ-radical are in very good agreement with those calculated by von Sonntag et al.[19] The combination of our ESR and theoretical studies (see also the Supporting Information) clearly point out the following: (a) The theoretically calculated HFCC values of 1-MeC iminyl σ-radical are in very good agreement with its experimentally observed HFCC values (Table 1), and this agreement justifies
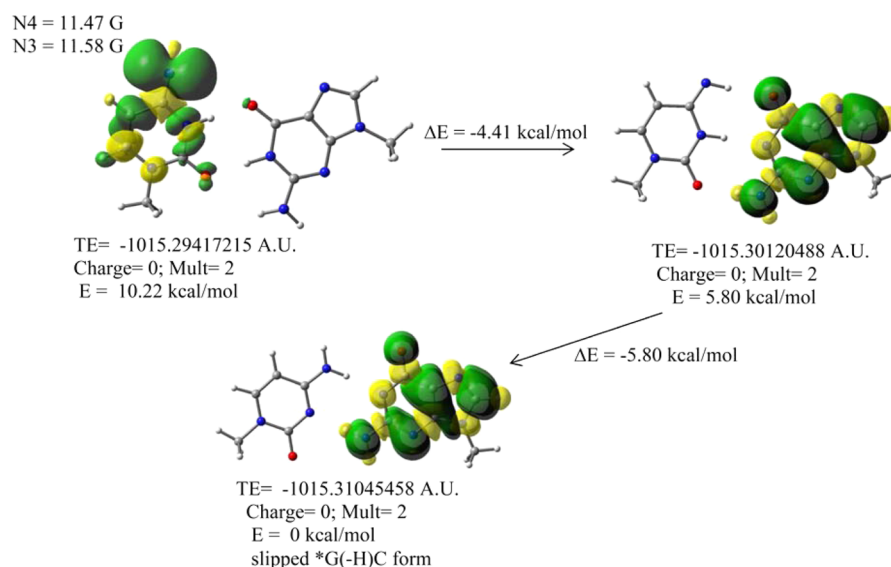
N4 = 11.47 G
N3 = 11.58 G

ΔE = -4.41 kcal/mol

TE= -1015.29417215 A.U.
Charge= 0; Mult= 2
E = 10.22 kcal/mol

TE= -1015.30120488 A.U.
Charge= 0; Mult= 2
E = 5.80 kcal/mol

ΔE = -5.80 kcal/mol

TE= -1015.31045458 A.U.
Charge= 0; Mult= 2
E = 0 kcal/mol
slipped *G(-H)C form

**Figure 3.** Proposed role of the cytosine iminyl $\sigma$-radical to produce neutral guanyl radical {G(N1−H)$^{\bullet}$:C [or *G(−H)C]}) via proton-coupled electron transfer in the one-electron-oxidized 9-Me-G:1-Me-C (the Me group at N9 in G and at N1 in C mimic sugar moieties). The calculations were performed by employing the $\omega$b97x/PCM/6-31++G(d) method for geometry optimization and spin density distribution plots (also see the Supporting Information, Figure S10). TE = total energy in atomic unit (A.U.). The HFCC values of N3 and N4 were shown for the 1-Me-C iminyl $\sigma$-radical (see left uppermost panel) in the one-electron-oxidized 9-Me-G:1-Me-C, and these values agree with those observed in the monomer (see Table 1).

the radical assignment of the spectra shown in Figure 1. Furthermore, experimental values of $A_{zz}$ components of the nitrogen hyperfine couplings owing to C(N4−H)$^{\bullet}$ are in good agreement with the theoretically calculated values. (b) Deprotonation from the N4 amine group in 1-MeC$^{\bullet+}$ at the syn site of the >C=O group at C2 with respect to the N4−H atom should aid the tautomeric formation of the iminyl $\sigma$-radical. This is evident from the relative stabilities of C(N4−H)$^{\bullet}_{syn}$ and C(N4−H)$^{\bullet}_{anti}$ (see Scheme 1 and the Supporting Information). (c) Our theoretical results show that iminyl $\sigma$-radical should not undergo deprotonation at N3, as the N3-deprotonated iminyl $\sigma$-radical is destabilized in solution by over 30 kcal/mol ($\Delta G = -32$ kcal/mol) over its conjugate acid (or the N3-protonated form) (see the Supporting Information). (d) As expected for a neutral $\pi$-radical such as C(N4−H)$^{\bullet}$, we find two axially symmetric anisotropic nitrogen HFCC values, whereas the iminyl $\sigma$-radical shows one anisotropic and one near isotropic nitrogen HFCC values (see Table 1 and Supporting Information, Figure S11).

*Role of Cytosine Iminyl $\sigma$-Radical in the Formation of Guanyl Radical in DNA.* Photolytically generated aminyl and iminyl radicals from arylhydrazones show DNA cleaving activity in aqueous solution (pH ca. 7) at ambient temperature.[49] In addition, the experimental and theoretical work by von Sonntag et al.[9,19] for the CW ESR spectrum of SO$_4^{\bullet-}$-induced one-electron-oxidized 1-MeC along with our results at low temperature (this work) clearly show that the C(N4−H)$^{\bullet}$ tautomerizes to the iminyl $\sigma$-radical in aqueous solution (pH ca. 7) at room temperature. Therefore, it would be of interest to investigate the role of cytosine iminyl $\sigma$-radical in the G:C base pair. On the basis of pulse radiolysis studies at ambient temperature in aqueous solution (pH ca. 7) of one-electron-oxidized calf thymus DNA, Anderson et al. has proposed cytosine iminyl $\sigma$-radical "gated" neutral guanyl radical [G(N1−H)$^{\bullet}$:C] formation (see Scheme 1 in ref 21). In lieu of this, we have employed the $\omega$b97x/6-31++G(d) method for geometry optimization to study the reaction energies along with the spin

density distribution plots for localization of the radical site of cytosine iminyl $\sigma$-radical in one-electron-oxidized G:C base pair. We have employed the integral equation formalism polarized continuum model (IEF-PCM) as implemented in Gaussian 09 to treat the effect of full solvent (see Materials and Methods).

Each radical species shown in the scheme by Anderson et al.[21] is designated as A, B, C, and D (see the Supporting Information, Figure S9). The reaction energy for the formation of radical B from radical A in the scheme proposed by Anderson et al.[21] is found to be endothermic (31.6 kcal/mol). The spin density distribution plots in each of the radicals A−D show that the unpaired spin (electron) is localized only on the guanine base in the one-electron-oxidized G:C base pair. Thus, these results clearly show that the mechanism proposed by Anderson et al.[21] is not energetically feasible. To resolve this issue, we have extensively searched for the most feasible reaction path that involves cytosine iminyl $\sigma$-radical "gated" [G(N1−H)$^{\bullet}$:C] formation as a modification of the mechanism proposed by Anderson et al. and have shown that in Figure 3 (see also the Supporting Information, Figure S10). The calculated reaction energy in each step is exothermic. The spin density distribution plots in radical B (the starting radical in Figure 3 and radical B in the Supporting Information, Figure S10) clearly show the cytosine iminyl $\sigma$-radical as an intermediate. The cytosine iminyl $\sigma$-radical gated [G(N1−H)$^{\bullet}$:C] is in the "slipped" form[34,54,55] and is ca. 10 kcal/mol more stable than the unslipped one-electron-oxidized G:C base pair involving authentic cytosine iminyl $\sigma$-radical (compare the nitrogen HFCC values with those in Table 1).

■ **CONCLUSION**

Our work has the following salient findings:
(i) The cytosine $\pi$-cation radical is shown to most favorably deprotonate in its ground state from the N4 exocyclic amine at the syn site of the >C=O group at C2 with respect to the N4−

H atom by producing the aminyl $\pi$-radical [C(N4−H)$^\bullet$]. C(N4−H)$^\bullet$ tautomerizes to form the iminyl $\sigma$-radical. The unusual nature of the $\sigma$-radical is that it is localized to an in-plane pure p-orbital of the exocyclic amine and shows large anisotropic $\alpha$-nitrogen coupling to N4 ($A_{zz}$ = 40 G) and an isotropic $\beta$-nitrogen coupling of 9.7 G to the cytosine ring nitrogen at N3. The nature of this species was earlier proposed by von Sonntag et al.,[19] and our work establishes this in an unequivocal fashion.

(ii) Under similar experimental conditions, deprotonation and subsequent tautomerization of the cytosine $\pi$-cation radical (Scheme 1, this work) prevails over the nucleophilic addition of hydroxyl anion (or water), as found for the thymine $\pi$-cation radical or its deprotonated form.[22] Thus, these results show that thymine and cytosine $\pi$-cation radical would undergo different reactions under similar conditions. The tautomerization of C(N4−H)$^\bullet$ to iminyl $\sigma$-radical has thus been observed in homogeneous glassy solution (this work) and in an aqueous solution at ambient temperature by von Sonntag et al.[19] However, there are experimental observations of hydration of C(N4−H)$^\bullet$ in aqueous solution at ambient temperature prevailing over its tautomerization to iminyl $\sigma$-radical; for example, 6-hydroxy-5,6-dihydrocytosin-5-yl radical has been observed to be the predominant radical via hydration of (N4−H)$^\bullet$ produced in a photosensitized reaction.[22,52,53]

(iii) Our theoretical calculations predict that the cytosine iminyl $\sigma$-radical could be formed in double-stranded DNA by the radiation-induced ionization−deprotonation process on cytosine that is only 10 kcal/mol above the lowest energy G:C radical form (slipped form of guanine N1-deprotonated G:C cation radical[34,54,55]). This is similar to the proposal of Anderson and co-workers,[21] who first suggested the cytosine iminyl $\sigma$-radical as an intermediate in DNA one-electron oxidation; however, our theoretical calculations provide an energy pathway that is lower than that obtained by the suggested proposal of Anderson et al.[21]

(iv) Our ESR studies suggest that several reactions of iminyl $\sigma$-radicals in cytosine monomers may occur, such as carbon-centered radical formation on the N1 side chain by deprotonation or by dimerization of the iminyl $\sigma$-radical itself. In addition, our results (Figures 1 and 2) at low temperature in homogeneous glassy solutions along with the studies of von Sonntag et al.[9,19] on SO$_4^{\bullet-}$-induced one-electron-oxidized 1-MeC in aqueous solution (pH ca. 7) point out that the cytosine $\pi$-cation radical deprotonates in the ground state from the exocyclic amine of the cytosine base (Scheme 1 and Supporting Information, Figure S8).

## ASSOCIATED CONTENT

**Ⓢ Supporting Information**

The Supporting Information is available free of charge on the ACS Publications website at DOI: 10.1021/acs.jpcb.5b05162.

(i) Estimated uncertainties (errors) in HFCC values; (ii) formation of iminyl $\sigma$-radical in one-electron-oxidized 1-Me-C in 7.5 M LiCl/H$_2$O; (iii) formation of iminyl $\sigma$-radical in one-electron-oxidized 1-Me-C in D$_2$O and in H$_2$O; (iv) formation of iminyl $\sigma$-radical in one-electron-oxidized 1-Me-C in 7.5 M LiCl/D$_2$O and its subsequent reaction via annealing at 170 K; (v) formation of iminyl $\sigma$-radical in one-electron-oxidized cidofovir in 7.5 M LiCl/D$_2$O and its subsequent reaction via annealing at 170 K at different concentrations of cidofovir; (vi)

formation of iminyl $\sigma$-radical in one-electron-oxidized cidofovir and in 1-MeC in 7.5 M LiCl/H$_2$O; (vii) formation of iminyl $\sigma$-radical in one-electron-oxidized 1-MeC, cidofovir, dCyd, and 5′-dCMP in 7.5 M LiCl/D$_2$O; (viii) comparison of ESR spectrum of iminyl $\sigma$-radical formed in 1-MeC with that of C1′$^\bullet$; (ix) proposed scheme of guanyl radical [G(N1−H)$^\bullet$:C] formation in the one-electron-oxidized 9-Me-G:1-Me-C (the Me group at N9 in G and at N1 in C mimic sugar moieties); (x) proposed role of the cytosine iminyl $\sigma$-radical to produce guanyl radical via proton coupled electron transfer in the one-electron-oxidized 9-Me-G:1-Me-C (the Me group at N9 in G and at N1 in C mimic sugar moieties); (xi) spin density distribution plots obtained employing the B3LYP/6-31G* method in B3LYP/6-31G* geometry optimized structures of 1-MeC $\pi$-cation radical, C(N4−H)$^\bullet_{anti}$, C(N4−H)$^\bullet_{syn}$, and 1-MeC iminyl $\sigma$-radical ;(xii) B3LYP/6-31G*-optimized structures of various radicals considered in this work and their isotropic and anisotropic HFCC values (PDF)

## AUTHOR INFORMATION

**Corresponding Authors**
*Am.A.: e-mail, adhikary@oakland.edu; phone, 248-370-2094; fax, 248-370-2321.
*M.D.S.: e-mail, sevilla@oakland.edu; phone, 248-370-2328; fax, 248-370-2321.

**Notes**
The authors declare no competing financial interest.

## ACKNOWLEDGMENTS

## REFERENCES

(1) Becker, D.; Adhikary, A.; Sevilla, M. D. The Role of Charge and Spin Migration in DNA Radiation Damage. In *Charge Migration in DNA: Physics, Chemistry and Biology Perspectives*; Chakraborty, T., Ed.; Springer-Verlag: Berlin, 2007; pp 139−175.

(2) Close, D. M. From the Primary Radiation Induced Radicals in DNA Constituents to Strand Breaks: Low Temperature EPR/ENDOR studies. In *Radiation-induced Molecular Phenomena in Nucleic Acids: A Comprehensive Theoretical and Experimental Analysis*; Shukla, M. K., Leszczynski, J., Eds.; Springer-Verlag: Berlin, 2008; pp 493−529.

(3) Bernhard, W. A. Radical Reaction Pathways Initiated by Direct Energy Deposition in DNA by Ionizing Radiation. In *Radical and Radical Ion Reactivity in Nucleic Acid Chemistry*; Greenberg, M. M., Ed.; John Wiley & Sons, Inc.: Hoboken, NJ, 2009; pp 41−68.

(4) Sagstuen, E.; Hole, E. O. Radiation Produced Radicals. In *Electron Paramagnetic Resonance*; Brustolon, G., Ed.; John Wiley & Sons, Inc.: Hoboken, NJ, 2009; pp 325−381.

(5) Becker, D.; Adhikary, A.; Sevilla, M. D. Mechanism of Radiation Induced DNA Damage: Direct Effects. In *Recent Trends in Radiation Chemistry*; Rao, B. S. M., Wishart, J., Eds.; World Scientific Publishing Co.: Singapore, 2010; pp 509−542.

(6) Becker, D.; Adhikary, A.; Sevilla, M. D. Physicochemical Mechanisms of Radiation Induced DNA Damage. In *Charged Particle and Photon Interactions with Matter—Recent Advances, Applications, and Interfaces*; Hatano, Y., Katsumura, Y., Mozumder, A., Eds.; CRC Press, Taylor & Francis Group: Boca Raton, FL, 2010; pp 503−541.

(7) Adhikary, A.; Becker, D.; Sevilla, M. D. Electron Spin Resonance of Radicals in Irradiated DNA. In *Applications of EPR in Radiation Research*; Lund, A., Shiotani, M., Eds.; Springer-Verlag: Berlin, 2014; pp 299−352.

(8) Adhikary, A.; Becker, D.; Palmer, B. J.; Heizer, A. N.; Sevilla, M. D. Direct Formation of The C5′-radical in The Sugar-phosphate Backbone of DNA By High Energy Radiation. *J. Phys. Chem. B* **2012**, *116*, 5900−5906.

(9) von Sonntag, C. *Free-Radical-Induced DNA Damage and Its Repair*; Springer-Verlag: Berlin, 2006; pp 213−482.

(10) Adhikary, A.; Kumar, A.; Becker, D.; Sevilla, M. D. Theory and ESR Spectral Studies of DNA-radicals. In *Encyclopedia of Radicals in Chemistry, Biology and Materials*; Chatgilialoglu, C., Struder, A., Eds.; John Wiley & Sons Ltd: Chichester, UK, 2012; pp 1371−1396.

(11) Steenken, S. Purine Bases, Nucleosides and Nucleotides: Aqueous Solution Redox Chemistry and Transformation Reactions of Their Radical Cations and e− and OH-adducts. *Chem. Rev.* **1989**, *89*, 503−520.

(12) Steenken, S. Electron-transfer-induced Acidity/Basicity and Reactivity Changes of Purine and Pyrimidine Bases. Consequences of Redox Processes for DNA Base Pairs. *Free Radical Res.* **1992**, *16*, 349−379.

(13) Steenken, S. Electron Transfer in DNA? Competition by Ultra-fast Proton Transfer? *Biol. Chem.* **1997**, *378*, 1293−1297.

(14) Cai, Z.; Sevilla, M. D.; Schuster, G. B. Studies of Excess Electron and Hole Transfers. *Top. Curr. Chem.* **2004**, *237*, 103−127.

(15) Kumar, A.; Sevilla, M. D. π- vs. σ-Radical States of One-electron-oxidized DNA/RNA Bases: A Density Functional Theory Study. *J. Phys. Chem. B* **2013**, *117*, 11623−11632.

(16) Bešić, E.; Sanković, K.; Gomzi, V.; Herak, J. N. Sigma Radicals in Gamma-irradiated Single Crystals of 2-Thiothymine. *Phys. Chem. Chem. Phys.* **2001**, *3*, 2723−2725.

(17) Sevilla, M. D.; Swarts, S. Electron Spin Resonance Study of Radicals Produced by One-electron Loss From 6-Azauracil, 6-Azathymine, and 6-Azacytosine. Evidence for Both σ and π Radicals. *J. Phys. Chem.* **1982**, *86*, 1751−1755.

(18) O'Neill, P.; Davies, S. E. Pulse Radiolytic Study of the Interaction of $SO_4^{•−}$ With Deoxynucleosides. Possible Implications for Direct Energy Deposition. *Int. J. Radiat. Biol.* **1987**, *52*, 577−587.

(19) Naumov, S.; Hildenbrand, K.; von Sonntag, C. Tautomers of the N-centered Radical Generated by Reaction of $SO_4^{•−}$ With N1-substituted Cytosines in Aqueous Solution. Calculation of Isotropic Hyperfine Coupling Constants by a Density Functional Method. *J. Chem. Soc., Perkin Trans. 2* **2001**, 1648−1653.

(20) Geimer, J.; Hildenbrand, K.; Naumov, S.; Beckert, D. Radicals Formed by Electron Transfer From Cytosine and 1-Methylcytosine to the Triplet State of Anthraquinone-2,6-disulfonic Acid. A Fourier-transform EPR Study. *Phys. Chem. Chem. Phys.* **2000**, *2*, 4199−4206.

(21) Anderson, R. F.; Shinde, S. S.; Maroz, A. Cytosine-gated Hole Creation and Transfer in DNA in Aqueous Solution. *J. Am. Chem. Soc.* **2006**, *128*, 15966−15967.

(22) Krishna, C. M.; Decarroz, C.; Wagner, J. R.; Cadet, J.; Riesz, P. Menadione Sensitized Photooxidation of Nucleic Acid and Protein Constituents. An ESR and Spin-trapping Study. *Photochem. Photobiol.* **1987**, *46*, 175−182.

(23) Adhikary, A.; Kumar, A.; Heizer, A. N.; Palmer, B. J.; Pottiboyina, V.; Liang, Y.; Wnuk, S. F.; Sevilla, M. D. Hydroxyl Ion Addition to One-electron Oxidized Thymine: Unimolecular Inter-conversion of C5 to C6 OH-adducts. *J. Am. Chem. Soc.* **2013**, *135*, 3121−3135.

(24) Khanduri, D.; Adhikary, A.; Sevilla, M. D. Highly Oxidizing Excited States of One-electron Oxidized Guanine in DNA: Wave-length and pH Dependence. *J. Am. Chem. Soc.* **2011**, *133*, 4527−4537.

(25) Adhikary, A.; Kumar, A.; Palmer, B. J.; Todd, A. D.; Heizer, A. N.; Sevilla, M. D. Reactions of 5-Methylcytosine Cation Radicals in DNA and Model Systems: Thermal Deprotonation From the 5-Methyl group vs. Excited State Deprotonation From Sugar. *Int. J. Radiat. Biol.* **2014**, *90*, 433−445.

(26) Adhikary, A.; Kumar, A.; Palmer, B. J.; Todd, A. D.; Sevilla, M. D. Formation of S-Cl Phosphorothioate Adduct Radicals in dsDNA-S-oligomers: Hole Transfer to Guanine vs. Disulfide Anion Radical Formation. *J. Am. Chem. Soc.* **2013**, *135*, 12827−12838.

(27) Adhikary, A.; Malkhasian, A. Y. S.; Collins, S.; Koppen, J.; Becker, D.; Sevilla, M. D. UVA-visible Photo-excitation of Guanine radical cations Produces Sugar Radicals in DNA and Model Structures. *Nucleic Acids Res.* **2005**, *33*, 5553−5564.

(28) Adhikary, A.; Collins, S.; Khanduri, D.; Sevilla, M. D. Sugar Radicals Formed by Photo-excitation of Guanine Cation Radical in Oligonucleotides. *J. Phys. Chem. B* **2007**, *111*, 7415−7421.

(29) Adhikary, A.; Kumar, A.; Becker, D.; Sevilla, M. D. The Guanine Cation Radical: Investigation of Deprotonation States by ESR and DFT. *J. Phys. Chem. B* **2006**, *110*, 24171−24180.

(30) Khanduri, D.; Collins, S.; Kumar, A.; Adhikary, A.; Sevilla, M. D. Formation of Sugar Radicals in RNA Model Systems and Oligomers via Excitation of Guanine Cation Radical. *J. Phys. Chem. B* **2008**, *112*, 2168−2178.

(31) Adhikary, A.; Kumar, A.; Khanduri, D.; Sevilla, M. D. The Effect of Base Stacking on The Acid-base Properties of The Adenine Cation Radical [A•+] in Solution: ESR and DFT Studies. *J. Am. Chem. Soc.* **2008**, *130*, 10282−10292.

(32) Adhikary, A.; Khanduri, D.; Kumar, A.; Sevilla, M. D. Photo-excitation of Adenine cation radical [A•+] in The Near UV-vis Region Produces Sugar Radicals in Adenosine and in Its Nucleotides. *J. Phys. Chem. B* **2008**, *112*, 15844−15855.

(33) Adhikary, A.; Khanduri, D.; Pottiboyina, V.; Rice, C. T.; Sevilla, M. D. Formation of Aminyl Radicals on Electron Attachment to AZT: Abstraction From the Sugar Phosphate Backbone vs. One-electron Oxidation of Guanine. *J. Phys. Chem. B* **2010**, *114*, 9289−9299.

(34) Adhikary, A.; Kumar, A.; Munafo, S. A.; Khanduri, D.; Sevilla, M. D. Prototropic Equilibria in DNA Containing One-electron Oxidized GC: Intra-duplex vs. Duplex to Solvent Deprotonation. *Phys. Chem. Chem. Phys.* **2010**, *12*, 5353−5368.

(35) Adhikary, A.; Kumar, A.; Rayala, R.; Hindi, R. M.; Adhikary, A.; Wnuk, S. F.; Sevilla, M. D. One-electron Oxidation of Gemcitabine and Analogs: Mechanism of Formation of C3′ and C2′ Sugar Radicals. *J. Am. Chem. Soc.* **2014**, *136*, 15646−15653.

(36) Frisch, M. J.; Trucks, G. W.; Schlegel, H. B.; Scuseria, G. E.; Robb, M. A.; Cheeseman, J. R.; Scalmani, G.; Barone, V.; Mennucci, B.; Petersson, G. A. et al. *Gaussian 09*; Gaussian, Inc.: Wallingford, CT, 2009.

(37) Raiti, M. J.; Sevilla, M. D. Density Functional Theory Investigation of The Electronic Structure and Spin Density Distribution in Peroxyl Radicals. *J. Phys. Chem. A* **1999**, *103*, 1619−1626.

(38) *GaussView*; Gaussian, Inc.: Pittsburgh, PA, 2003.

(39) Tomasi, J.; Mennucci, B.; Cammi, R. Quantum Mechanical Continuum Solvation Models. *Chem. Rev.* **2005**, *105*, 2999−3093.

(40) Chai, J.-D.; Head-Gordon, M. Systematic Optimization of Long-range Corrected Hybrid Density Functionals. *J. Chem. Phys.* **2008**, *128*, 084106.

(41) Chai, J.-D.; Head-Gordon, M. Long-range Corrected Hybrid Density Functionals With Damped Atom−atom Dispersion Correc-tions. *Phys. Chem. Chem. Phys.* **2008**, *10*, 6615−6620.

(42) Kumar, A.; Sevilla, M. D. Proton Transfer Induced SOMO-to-HOMO Level Switching in One-electron Oxidized A-T and G-C Base Pairs: A Density Functional Theory Study. *J. Phys. Chem. B* **2014**, *118*, 5453−5458.

(43) De Clercq, E. The Acyclic Nucleoside Phosphonates From Inception to Clinical Use: Historical Perspective. *Antiviral Res.* **2007**, *75*, 1−13.

(44) Snoeck, R.; Sakuma, T.; De Clercq, E.; Rosenberg, I.; Holy, A. S)-1-(3-Hydroxy-2-phosphonylmethoxypropyl)cytosine, A Potent and Selective Inhibitor of Human Cytomegalovirus Replication. *Anti-microb. Agents Chemother.* **1988**, *32*, 1839−1844.

(45) Baik, M.-H.; Silverman, J. S.; Yang, I. V.; Ropp, P. A.; Szalai, V. S.; Thorp, H. H. Using Density Functional Theory to Design DNA Base Analogues With Low Oxidation Potentials. *J. Phys. Chem. B* **2001**, *105*, 6437−6444.

(46) Close, D. M. Calculated pKa's of The DNA Base Radical Ions. *J. Phys. Chem. A* **2013**, *117*, 473−480.

(47) Kolano, C.; Bucher, G.; Wenk, H. H.; Jäger, M.; Schade, O.; Sander, W. Photochemistry of 9-Fluorenone Oxime Phenylglyoxylate: A Combined TRIR, TREPR and ab initio Study. *J. Phys. Org. Chem.* **2004**, *17*, 207−214.

(48) Griller, D.; Mendenhall, G. D.; Van Hoof, W.; Ingold, K. U. Kinetic Applications of Electron Paramagnetic Resonance Spectroscopy. XV. Iminyl Radicals. *J. Am. Chem. Soc.* **1974**, *96*, 6068−6070.

(49) Portela-Cubillo, F.; Alonso-Ruiz, R.; Sampedro, D.; Walton, J. C. 5-*Exo*-cyclizations of Pentenyliminyl Radicals: Inversion of The *Gem*-dimethyl Effect. *J. Phys. Chem. A* **2009**, *113*, 10005−10012.

(50) Hwu, J. R.; Lin, C. C.; Chuang, S. H.; King, K. Y.; Su, T.-R.; Tsay, S.-C. Aminyl and Iminyl Radicals From Arylhydrazones in The Photo-induced DNA Cleavage. *Bioorg. Med. Chem.* **2004**, *12*, 2509−2515.

(51) Labet, V.; Grand, A.; Cadet, J.; Eriksson, L. A. Deamination of The Radical Cation of The Base Moiety of 2′-Deoxycytidine: A Theoretical Study. *ChemPhysChem* **2008**, *9*, 1195−1203.

(52) Decarroz, C.; Wagner, J. R.; van Lier, J. E.; Krishna, C. M.; Riesz, P.; Cadet, J. Sensitized Photo-oxidation of Thymidine by 2-Methyl-1,4-naphthoquinone. Characterization of The Stable Photoproducts. *Int. J. Radiat. Biol.* **1986**, *50*, 491−505.

(53) Wagner, J. R.; Cadet, J. Oxidation Reactions of Cytosine DNA Components by Hydroxyl Radical and One-electron Oxidants in Aerated Aqueous Solutions. *Acc. Chem. Res.* **2010**, *43*, 564−571.

(54) Reynisson, J.; Steenken, S. DNA-base Radicals. Their Base Pairing Abilities As Calculated by DFT. *Phys. Chem. Chem. Phys.* **2002**, *4*, 5346−5352.

(55) Bera, P. P.; Schaefer, H. F., III (G-H)•−C and G−(C-H)• Radicals Derived From The Guanine.Cytosine Base Pair Cause DNA Subunit Lesions. *Proc. Natl. Acad. Sci. U. S. A.* **2005**, *102*, 6698−6703.